Computational Materials Science 246 (2025) 113342

Contents lists available at ScienceDirect

Computational Materials Science

journal homepage: www.elsevier.com/locate/commatsci

Letter

Edge- and vertex-originated differences between nanoparticles and nanovoids: A density functional theory study of face-centered-cubic Al

Akio Ishii

Department of Mechanical Science and Bioengineering, Osaka University, 1-3 Machikaneyama-cho, Toyonaka, Osaka 560-8531, Japan

ARTICLE INFO

Keywords:
Nanoparticle
Nanovoid
Atomistic simulation
Density functional theory

ABSTRACT

The differences between nanoparticles and nanovoids cannot be clearly distinguished energetically using conventional comparisons based on the surface energies of these species. For example, nanoparticles and nanovoids with the same volume and shape are considered energetically equivalent to the conventional Wulff construction, and so the difference in their morphology cannot be evaluated. This can be attributed to fact that using such approaches, the effects of excess defects, edges, and vertices in nanoparticles and nanovoids are typically ignored. In this study, we investigated the energetic differences between face-centered-cubic (FCC) nanoparticles of Al and nanovoids in bulk FCC Al structure with conventional truncated octahedral shapes by calculating the excess energies attributed to their edges, vertices, and sizes. This was achieved using density functional theory calculations and our previously reported method for evaluating the effects of edges and vertices. The morphological differences between the nanoparticles and nanovoids were also discussed based on the obtained results.

1. Introduction

Nanoparticles are promising nanoscale materials that exhibit unique properties that differ from those of bulk metals, and extensive research has been conducted to develop nanoparticles with desirable characteristics [1–4]. On the other hand, the formation of nanovoids in structural materials has also been studied in detail [5–7] due to the negative effects that nanovoids impart on the mechanical properties of materials, causing embrittlement and blistering under hydrogen rich conditions [8–13]. Such nanovoids are often observed in nuclear materials induced by the irradiation [14–16]. The energetic differences between nanoparticles and nanovoids have not yet been thoroughly investigated since these components are usually studied individually by researchers working in different fields. Through our several-years cross-field studies, we realized that the differences between nanoparticles and nanovoids cannot be energetically distinguished by conventional surface energy comparisons. For example, nanoparticles and nanovoids with the same volume and shape are considered energetically equivalent to the conventional Wulff construction [17]; the differences in their morphologies cannot be evaluated since the conventional Wulff construction ignores the effects of excess defects, edges, and vertices in these structures [18]. Thus, the main objective of this study is to understand the energetic difference between nanoparticles and nanovoids by investigating the effects of edges and vertices on their excess energies compared to the bulk energy. It is expected that the obtained results will aid in the discussion of their morphologies [19].

More specifically, considering Al element, the energetic difference between face-centered-cubic (FCC) nanoparticles and nanovoids in FCC structures with conventional truncated octahedral shapes (i.e., containing {111} and {100} faces) is evaluated [18,19]. The edge and vertex energies of the nanoparticles and nanovoids are calculated with respect to the size using the density functional theory (DFT) approach combined with a method for evaluating the effect of edges and vertices, as proposed previously by us [18]. Subsequently, the differences in the morphologies of these structures are discussed. The excess energies attributed to the edges and vertices are denoted as the "edge" and "vertex" energies in the following for the convenience [18]. Note that Al was selected for analysis to reduce the calculation cost.

2. Calculation of the edge energy

Based on our previous study [18], the edge energies of conventional truncated octahedral FCC nanoparticles and nanovoids with {111} and {100} faces were calculated using two-dimensional (2D) atomic model sets, as shown in Fig. 1. Each set included two atomic models for calculation of the edge energies of FCC nanoparticles and nanovoids of the same size and shape, as presented in Fig. 2. This atomic model describes the edges of the larger nanoparticles and nanovoids as the index of the set increases from I to IV. All 2D models consist of hexagonal prisms with two {111}/{111} and four {111}/{100} edges,

E-mail address: ishii@me.es.osaka-u.ac.jp.

https://doi.org/10.1016/j.commatsci.2024.113342
Received 6 August 2024; Received in revised form 1 September 2024; Accepted 2 September 2024

in addition to an infinite length along the longitudinal direction z. The thickness of the unit cell along the z direction is only two $(\bar{1}10)$ atomic layers owing to the periodicity along the z direction. The {111}/{111} and {111}/{100} edges correspond to those of conventional truncated octahedral FCC nanoparticles and nanovoids, although no vertices exist owing to the periodicity along the z direction. Thus, the effects of the edges and vertices can be distinguished, and the edge energy of a nanoparticle or nanovoid can be defined as follows [18]:

$$\Delta E^{\mathrm{edge}} \equiv \frac{1}{a_z^{2\mathrm{D}}}\left(E^{2\mathrm{D}} - N^{2\mathrm{D}}E^{\mathrm{bulk}} - \gamma^{\{111\}}A^{2\mathrm{D}}_{\{111\}} - \gamma^{\{100\}}A^{2\mathrm{D}}_{\{100\}}\right). \quad (1)$$

where $E^{2\mathrm{D}}$ denotes the potential energy of the 2D atomic model for the optimized atomic structures calculated using the DFT approach, E^{bulk} denotes the bulk energy (per atom) of a material without a surface, $\gamma^{\{111\}}$ and $\gamma^{\{100\}}$ denote the surface energies of the {111} and {100} faces, respectively, and $a_z^{2\mathrm{D}}$ denotes the unit cell thickness. In addition, $N^{2\mathrm{D}}$ denotes the number of atoms in the 2D atomic model, while $A^{2\mathrm{D}}_{\{111\}}$ and $A^{2\mathrm{D}}_{\{100\}}$ denote the {111} and {100} surface areas in the 2D atomic model. It should be noted here that $N^{2\mathrm{D}}$ does not indicate the size of the nanovoid, nor the number of vacancies inside the nanovoids. We consider that the size effect in the edge energy is due to the distance between the edges in this modeling. The values of E^{bulk}, $\gamma^{\{111\}}$, and $\gamma^{\{100\}}$ were obtained from the Materials Project database as −3.75 eV/atom, 0.048, and 0.057 eV/Å^2, respectively [20].

The Vienna Ab initio Simulation Package was used for the DFT atomistic simulations [21]. Electron–ion interactions were described using the projector-augmented wave method [22]. In addition, the exchange correlation between the electrons was treated using the Perdew–Burke–Ernzerhof generalized gradient approximation [23] with an energy cutoff of 520 eV for the plane-wave basis set. The energy convergence criteria for the electronic and ionic structure relaxations were set to 1.0×10^{-6} and 1.0×10^{-3} eV, respectively. The size of the supercell was set to $50 \times 50 \times 2.88$ Å to describe the vacuum around the faces on xy-plane for a nanoparticle. $56.6 \times 52.0 \times 2.88$ Å supercells with bulk FCC structures surrounding the nanovoid were uniformly used for all nanovoids of different sizes. $1 \times 1 \times 8$ k-point and $3 \times 3 \times 8$ k-point meshes was used for the nanoparticles and nanovoids, respectively. The value of $E^{2\mathrm{D}}$ for each atomic model was calculated after structural optimization, including the relaxation of cell length along the z-direction for the nanoparticles and the whole-cell shape for the nanovoids. It was confirmed that the extra interactions of the surfaces had no significant effects on these calculations owing to the finite supercell size: the periodicity of the atomic models. Note that the temperature effect was not considered in the calculation due to the calculation cost; our atomic models are too large to implement dynamic sampling or phonon analysis using DFT calculation.

Table 1 lists the calculated ΔE^{edge} values for each set. From the ΔE^{edge} values obtained for the nanoparticles, it can be seen that a large edge energy exists even in small nanoparticles, and this energy increases as the size of the atomic model (i.e., the index) increases and saturates for the III and IV sets, that is similar trend to those of the nanoparticles examined in our previous study [18]. On the other hand, the edge energy of a nanovoid is smaller than that of a nanoparticle of the same size, and even becomes negative for small nanovoids. However, it increases drastically as the size increases, and never saturates in the size range investigated herein. This indicates that, in contrast to nanoparticles, nanovoids cannot grow significantly, maintaining their truncated octahedral shape. The coexistence of multiple small nanovoids or planar-like shapes are suggested to stabilize the nanovoids in FCC Al metal. This may partly account for the fact that 2D crack-type defects are usually observed in metals on a large scale. Three-dimensional (3D) shapes are not favored chemically because of the excess energy associated with their edges, although the gases inside the voids or cracks tend to impart elastic stabilization on the spherical shapes [24,25]. Thus, the large-scale spherical nanovoids may be only stable under the existence of gases inside them.

Table 1
Calculated edge energies ΔE^{edge} for the atomic model sets shown in Fig. 1. The units are eV/Å. The size indicates the number of atoms (vacancies) of the nanoparticle (nanovoid) in the set.

Set	Size	Nanoparticle	Nanovoid
I	14	0.69	−0.085
II	43	0.75	0.088
III	88	0.94	0.252
IV	149	0.97	0.410

3. Calculation of the vertex energy

Using the calculated ΔE^{edge} values and the potential energies of the actual 3D truncated octahedral atomic models of nanoparticles or nanovoids with identical edge lengths a ($E^{3\mathrm{D}}$), the vertex energy $\Delta E^{\mathrm{vertex}}$ was calculated. Since such truncated octahedra possess 12 {111}/{111} and 24 {111}/{100} edges, the vertex energy $\Delta E^{\mathrm{vertex}}$ was obtained from $E^{3\mathrm{D}}$ and ΔE^{edge} to cancel the edge effect, as follows [18]:

$$\Delta E^{\mathrm{vertex}} \equiv \frac{1}{24}\left(E^{3\mathrm{D}} - N^{3\mathrm{D}}E^{\mathrm{bulk}} - 6\Delta E^{\mathrm{edge}}a - \left(12\sqrt{3}\gamma^{\{111\}} + 6\gamma^{\{100\}}\right)a^2\right). \quad (2)$$

where $N^{3\mathrm{D}}$ denotes the number of atoms in the 3D atomic model, $12\sqrt{3}a^2$ and $6a^2$ indicate the total areas of the {111} and {100} faces of the truncated octahedron, respectively, and 24 corresponds to the number of vertices in the truncated octahedron. To investigate the size effect, atomic model sets (I–IV) were constructed that included differently sized 3D truncated octahedral nanoparticles and nanovoids, as shown in Fig. 2. For this purpose, the nanoparticles and nanovoids in the same sets were of the same size. These sets were paired with the 2D atomic model sets shown in Fig. 1, and the distances between the edges of the truncated octahedra in each set were consistent with those in the 2D atomic model set with the same index. Thus, the corresponding value of ΔE^{edge} in Table 1 was used to calculate $\Delta E^{\mathrm{vertex}}$. We consider that the size effect in the vertex energy is due to the distance between the vertices (the length of the edges) in this modeling. It should be noted here that only the atomic model of a nanoparticle is included in set IV because of the limitations of our computational resources; the corresponding atomic model of a nanovoid was found to be too large to allow calculation of the potential energy, even when high-performance supercomputers were employed.

For the detail of the atomic models and the DFT parameters, the supercell of nanoparticles was set to $50 \times 50 \times 50$ Å to describe the vacuum around the nanoparticles, and a $1 \times 1 \times 1$ k-point mesh was used. No periodicity was assumed in the atomic models of the nanoparticles. $[100] \times [010] \times [001] = 24.2 \times 24.2 \times 24.2$, $28.1 \times 28.1 \times 2.81$, and $36.2 \times 36.2 \times 36.2$ Å supercells with FCC bulk structures surrounding the nanovoids were used for the nanovoids in sets I, II, and III, respectively, avoiding surface interactions due to the periodicity of the atomic models. A $3 \times 3 \times 3$ k-point mesh was used for all nanovoids. For each atomic model, the value of $E^{3\mathrm{D}}$ was calculated after structural optimization (including the relaxation of cell shapes of the nanovoids). All other DFT parameters were the same as those described in the previous section.

Table 2 lists the calculated vertex energies $\Delta E^{\mathrm{vertex}}$ with respect to the sizes of the nanoparticles and the nanovoids. The percentages of the surface, edge, and vertex energies that contributed to the total excess energies of the nanoparticles and nanovoids (i.e., the energy increment compared to the bulk FCC Al) are also shown in Table 3. The negative percentages correspond to the negative excess energies of the edges and vertices in Tables 1 and 2.

It can be seen that the value of $\Delta E^{\mathrm{vertex}}$ decreases with an increase in the nanoparticle size, which is consistent with our previous study [18]. Interestingly, it can be seen from Table 2 that this value eventually becomes negative. In addition, from Table 3, it is evident that although

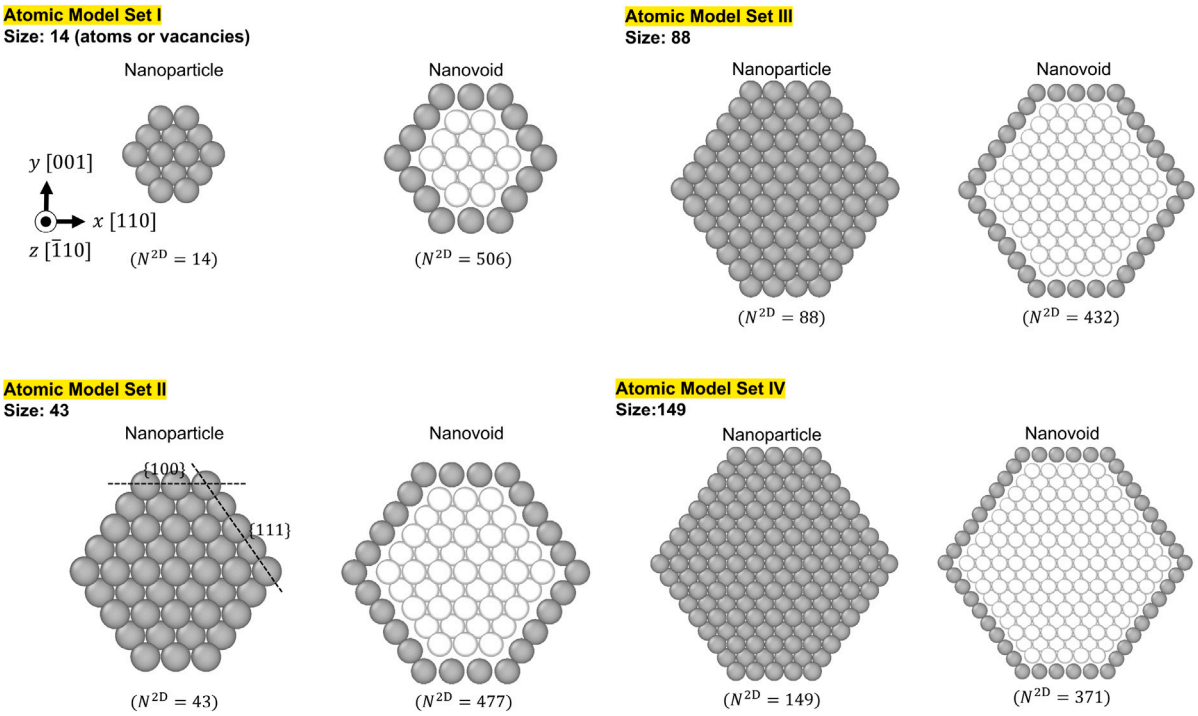

Fig. 1. 2D Atomic model sets (from I to IV) for calculation of the edge energies ΔE^{edge} of nanoparticles and nanovoids with different sizes. The thickness of the unit cell along the z direction is two $(\bar{1}10)$ atomic layers for all models. White circles indicate the positions of vacancies in the nanovoids. Only the atoms surrounding the 2D nanovoids are shown for the atomic models (i.e., atoms with different coordination numbers from those in FCC bulk structure). The atomic structures were visualized using OVITO software [26].

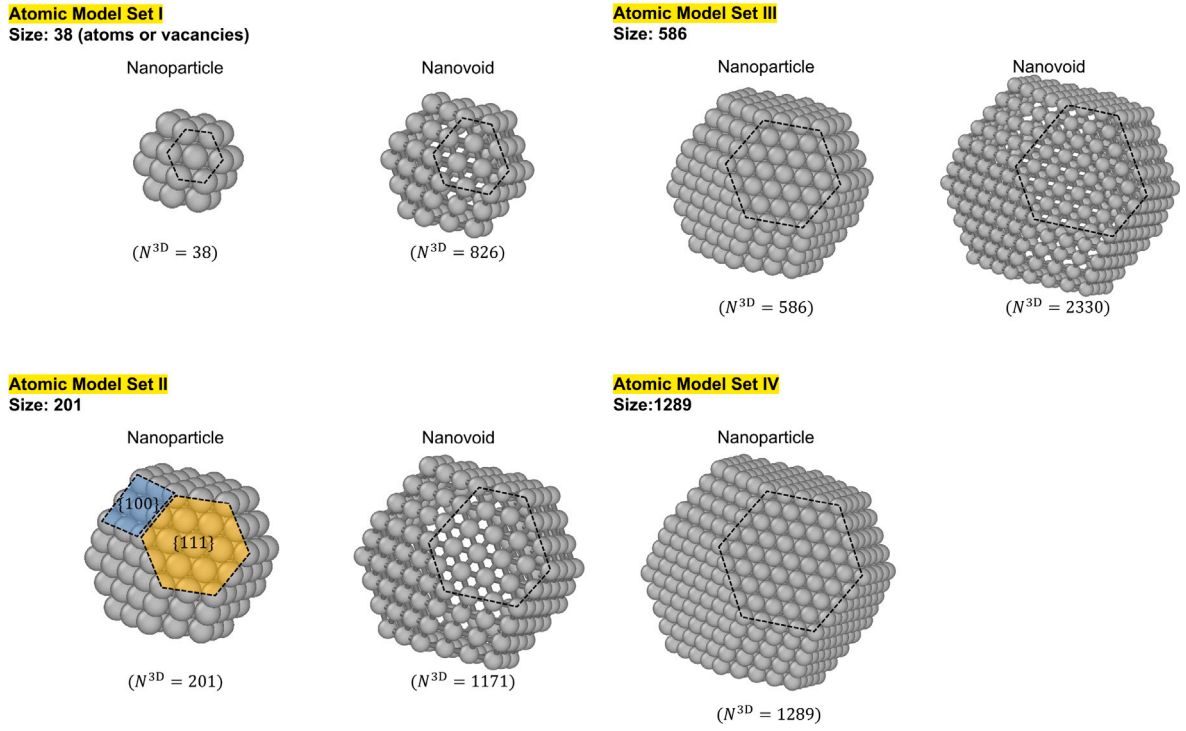

Fig. 2. 3D Atomic model sets (from I to IV) for calculation of the vertex energies ΔE^{vertex} of the nanoparticles and nanovoids with different sizes. Only the atoms surrounding the nanovoid are shown for the nanovoid atomic models. The bonds in the nanovoids are provided as guides to easily understand the shapes. The broken lines are provided as guides to the eyes for the {111} face. Note that the atoms surrounding the nanovoid do not construct hexagonal {111} faces with the *ideal* edge lengths; however, the nanovoid itself does construct such faces. The atomic structures were visualized using OVITO software [26].

Table 2
Calculated vertex energy ΔE^{vertex} for each atomic model set in Fig. 2. The units are eV (per vertex). The size indicates the number of atoms (vacancies) in the nanoparticles (nanovoids) in each set.

Set	Size	Nanoparticle	Nanovoid
I	38	0.09	0.28
II	201	−0.07	0.38
III	586	−0.27	0.18
IV	1289	−0.49	–

Table 3
Fractions of the surface, edge, and vertex energies in the total excess energy of a nanoparticle. The units are %, and the negative percentages reflect the negative excess energies of the edges and vertices given in Tables 1 and 2.

Set	Surface	Edge	Vertex
Nanoparticle			
I	43	48	9
II	64	39	−3
III	70	35	−5
IV	76	29	−5
Nanovoid			
I	66	−9	43
II	77	6	17
III	85	11	4

the percentage decreased as the nanoparticle size increased, the edge energy still occupied a large percentage of the total excess energy, on the other hand, the percentage of the vertex energy was extremely small or even negative. Considering that the sphere can be considered as a shape with infinite vertices and no edges, the obtained result indicates that during growth, the nanoparticles become more spherical, even avoiding becoming planar, thereby agreeing with previous experimental reports [27,28]. Notably, this appears to be the first time that the spherical nanoparticles have been considered to be energetically stable, despite the fact that they are always observed experimentally. The planar shape becomes the most energetically stable state if only the surface energy is considered when discussing the morphology; this can be attributed to the orientation dependency of the surface energy. Although classical nucleation theory (CNT) tells us that the sphere is the most stable shape because it has a minimum surface area [29], CNT approximates the surface energy as a constant value and the excess energy due to the difference of the crystal orientation, which must exist for the spherical shape, is not considered. Our study suggests that this excess energy due to the difference of the orientation is compensated by the negative vertex energy, keeping the spherical shape of the nanoparticles stable.

On the other hand, the value of ΔE^{vertex} is always positive for nanovoids, and is relatively high even for small nanovoids, as indicated in Table 2. It can also be seen that the percentage contribution of the vertex energy is quite high, although that of the edge energy is negative for small nanovoids (set I). As the nanovoid size increases, the percentage of the edge energy increases and becomes significant, although the vertex energy becomes negligible, as shown in Table 3. This indicates that the nanovoids nucleate in the form of a coin, decreasing the number of vertices and increasing the edge length. Subsequently, the nanovoids grow like planar cracks or spherical voids, decreasing the length of each edge. The value of ΔE^{vertex} initially increases and then decreases for nanovoids; thus, a maximum value exists for ΔE^{vertex} with respect to the nanovoid size. We think this is due to the interactions between vertices and the pair interactions between vacancies were also examined with respect to the distance between the vacancies, considering that vacancies instead of atoms exist at the nanovoid vertices; as detailed in the Appendix. And actually, a maximum of the pair interaction energy of vacancies with respect to the distance between the vacancies was detected. The above results therefore suggest that the Al nanovoids have a critical size of approximately 200 vacancies, after which they may change their morphology to become more spherical owing to a decrease in the vertex energy. It should be noted here that only the chemical effect was considered due to the surface morphologies of the nanovoids, and the morphology was also affected elastically by the gases present inside the voids (as mentioned above) and by the application of an external load [24,30,31].

4. Summary

In this study, the energetic difference between FCC nanoparticles of Al and nanovoids present in FCC Al with conventional truncated octahedral shapes were investigated by calculating the excess energies caused by the edges and vertices for species of different sizes. For this purpose, DFT calculations were employed in combination with a method for evaluating the effects of edges and vertices, as described in our previous work. The morphological differences between the nanoparticles and nanovoids were then discussed based on the obtained results. It was found that the Al nanoparticles nucleated and grew into spherical shapes owing to the large positive excess energy associated with the edges. However, the nanovoids in the bulk FCC Al nucleated in the form of coins owing to the negative excess energy of the edges and the large positive energy of the vertices. Subsequently, the nanovoids grew to generate planar cracks or spherical voids owing to the increased edge energy and the decreased vertex energy. Notably, although only the effects of the edges and vertices due to the connection of {111} and {100} faces were investigated, and the shapes of the nanoparticles and nanovoids were limited to conventional truncated octahedrons due to the limitations in calculation costs in this study, it was considered that these observations could be generalized because they agree with conventional experimental observations. Additionally, our method should be applicable to investigation of the excess edge and vertex energies at the interfaces of coherent precipitates in other materials. However, it will be necessary to distinguish between the chemical and elastic effects in such cases due to the presence of misfit strains between the atomic structures of the bulk and the precipitate using proper method [32–34].

CRediT authorship contribution statement

Akio Ishii: Writing – review & editing, Writing – original draft, Visualization, Validation, Methodology, Investigation, Funding acquisition, Formal analysis, Data curation, Conceptualization.

Declaration of competing interest

The authors declare that they have no known competing financial interests or personal relationships that could have appeared to influence the work reported in this paper.

Data availability

Data will be made available on request.

Acknowledgments

This study was partially supported by a Grant -in-Aid for Scientific Research (C) 21K03771 from the Japan Society for the Promotion of Science (JSPS). The DFT simulations were partly performed using the SQUID large-scale computer systems at the Cybermedia Center, Osaka University, and the MASAMUNE-IMR system at the Center for Computational Materials Science (Institute for Materials Research, Tohoku University, Japan).

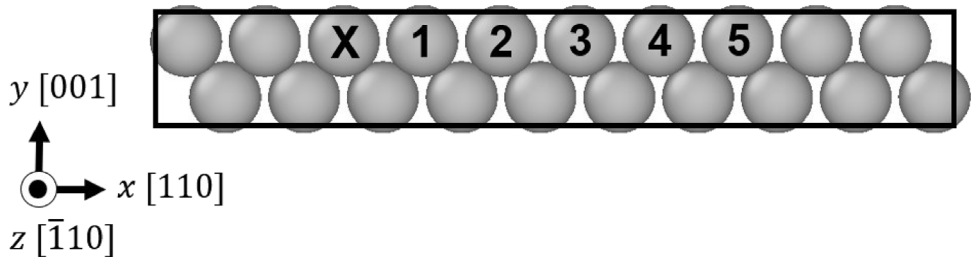

Fig. A.1. The atomic model used to investigate the pair interactions between the vacancies (40 atoms). The black lines indicate the supercell. The thickness of the unit cell along the z direction is four ($\bar{1}10$) atomic layers. A vacancy was fixed at position X, and the position of the second vacancy was varied between positions 1 and 5, that are in same ($\bar{1}10$) layer as the vacancy at position X. The atomic structures were visualized using OVITO software [26].

Table A.1
Calculated potential energy for each vacancy position shown in Fig. A.1. The standard of the potential energy was set to that obtained for position 1. The units are eV.

Position	Potential energy
1	0.00
2	0.10
3	0.12
4	0.05
5	0.02

Appendix. Pair interaction energies of the vacancies in Al

To investigate the origin of the critical value of ΔE^{vertex} with respect to the nanovoid size (see Section 3), the pair interactions of the vacancies were investigated with respect to the distance between the vacancies, considering that vacancies instead of atoms exist at the nanovoid vertices. As shown in Fig. A.1, atomic models based on 40 atoms without any vacancies were employed. By fixing a vacancy at the X position, the position of another vacancy was changed along the [110] direction from positions 1 to 5, and the potential energy was calculated in each case. A $1 \times 6 \times 6$ k-point mesh was used, and the potential energies were calculated after structural optimization, including the relaxation of the cell shape. All other DFT parameters were as described in the main text. Table A.1 lists the calculated potential energies at the various positions, wherein it can be seen that the maximum value were expected around positions 2 and 3. The distance between positions X and 2 was consistent with the distance between the vertices in set II, which has the maximum of the vertex energy (see Fig. 2 in the main text).

References

[1] C.M. Welch, R.G. Compton, The use of nanoparticles in electroanalysis: A review, Anal. Bioanal. Chem. 384 (2006) 601–619.
[2] V. Mohanraj, Chen, Nanoparticles-a review, Trop. J. Pharm. Res. 5 (2006) 561–573.
[3] R. Ferrando, J. Jellinek, R.L. Johnston, Nanoalloys: From theory to applications of alloy clusters and nanoparticles, Chem. Rev. 108 (2008) 845–910.
[4] N. Nakamura, K. Matsuura, A. Ishii, H. Ogi, Restructuring in bimetallic core-shell nanoparticles: Real-time observation, Phys. Rev. B 105 (2022) 125401.
[5] W. Geng, L. Wan, J.-P. Du, A. Ishii, N. Ishikawa, H. Kimizuka, S. Ogata, Hydrogen bubble nucleation in α-iron, Scr. Mater. 134 (2017) 105–109.
[6] J.-P. Du, W.T. Geng, K. Arakawa, J. Li, S. Ogata, Hydrogen-enhanced vacancy diffusion in metals, J. Phys. Chem. Lett. 11 (2020) 7015–7020.
[7] K. Arakawa, A. Kageyama, H. Hiroshima, H. Yasuda, S. Ogata, Hydrogen effects on the migration of nanoscale cavities in iron, ISIJ Inter. 61 (2021) 2305–2307.
[8] C.A. Zapffe, C.E. Sims, Internal stress and defects in steel, Trans. AIME 145 (1941) 225–261.
[9] J.B. Condon, T. Schober, Hydrogen bubbles in metals, J. Nucl. Mater. 207 (1993) 1–24.
[10] A. Griesche, E. Dabah, T. Kannengiesser, N. Kardjilov, A. Hilger, I. Manke, Three-dimensional imaging of hydrogen blister in iron with neutron tomography, Acta Mater. 78 (2014) 14–22.
[11] M.C. Tiegel, M.L. Martin, A.K. Lehmberg, M. Deutges, C. Borchers, R. Kirchheim, Crack and blister initiation and growth in purified iron due to hydrogen loading, Acta Mater. 115 (2016) 24–34.
[12] X. Tao, G.C. Lv, J. Kou, X. Xiong, A.A. Volinsky, C.S. Ku, K. Chen, Y.J. Su, Synchrotron X-ray Laue diffraction study of hydrogen-induced blisters on iron grain boundaries, Scr. Mater. 169 (2019) 82–86.
[13] W.Q. Chen, X.Y. Wang, K.L. Li, Y.N. Wang, T.W. Morgan, B. Xu, Y.L. Chiu, W. Liu, Nucleation mechanism of intra-granular blisters in tungsten exposed to hydrogen plasma, Scr. Mater. 187 (2020) 243–249.
[14] T. Ohshima, A. Uedono, K. Abe, H. Itoh, Y. Aoki, M. Yoshikawa, S. Tanigawa, I. Nashiyama, Characterization of vacancy-type defects and phosphorus donors introduced in 6H-SiC by ion implantation, Appl. Phys. A 67 (1998) 407–412.
[15] Y.-R. Lin, C.-S. Ku, C.-Y. Ho, W.-T. Chuang, S. Kondo, J.-J. Kai, Irradiation-induced microstructural evolution and swelling of 3C-SiC, J. Nucl. Mater. 459 (2015) 276–283.
[16] K.Y. Fung, Y.R. Lin, P.J. Yu, J.J. Kai, A. Hu, Microscopic origin of black spot defect swelling in single crystal 3C-SiC, J. Nucl. Mater. 508 (2018) 292–298.
[17] G. Wulff, XXV. Zur Frage der Geschwindigkeit des Wachsthums und der Auflösung der Krystallflächen, Z. Kristall. 34 (1901) 449–530.
[18] A. Ishii, Energetical effects of the edges and vertices of face-centered-cubic Pd and Au nanoparticles: A density functional theory study, Comput. Mater. Sci. 243 (2024) 113122.
[19] A. Ishii, N. Nakamura, Ab initio morphology prediction of Pd, Ag, Au, and Pt nanoparticles on (0001) sapphire substrates, J. Appl. Phys. 135 (2024) 094301.
[20] A. Jain, S.P. Ong, G. Hautier, W. Chen, W.D. Richards, S. Dacek, S. Cholia, D. Gunter, D. Skinner, G. Ceder, et al., Commentary: The Materials Project: A materials genome approach to accelerating materials innovation, APL Mater. 1 (2013) 011002.
[21] G. Kresse, J. Furthmüller, Efficient iterative schemes for ab initio total-energy calculations using a plane-wave basis set, Phys. Rev. B 54 (1996) 11169–11186.
[22] G. Kresse, D. Joubert, From ultrasoft pseudopotentials to the projector augmented-wave method, Phys. Rev. B 59 (1999) 11–19.
[23] J. Perdew, K. Burke, M. Ernzerhof, Generalized gradient approximation made simple, Phys. Rev. Lett. 77 (1996) 3865–3868.
[24] A. Ishii, Influence of elastic anisotropy on the shapes of ellipsoidal blisters and stress field around the blisters in solid materials, AIP Adv. 13 (2023) 125024.
[25] T. Mura, Micromechanics of Defects in Solids, Springer Science & Business Media, 2013.
[26] A. Stukowski, Visualization and analysis of atomistic simulation data with OVITO-the Open Visualization Tool, Model. Sim. Mater. Sci. Eng. 18 (2010) 015012.
[27] R. Narayanan, M.A. El-Sayed, Catalysis with transition metal nanoparticles in colloidal solution: Nanoparticle shape dependence and stability, J. Phys. Chem. B 109 (2005) 12663–12676.
[28] Y. Li, Q. Liu, W. Shen, Morphology-dependent nanocatalysis: Metal particles, Dalton Trans. 40 (2011) 5811–5826.
[29] V.I. Kalikmanov, Classical Nucleation Theory, Springer, 2012.
[30] A. Ishii, Morphology prediction of elastically interacting Zr hydride precipitates and cracks in α-Zr using atomistically informed Eshelby's ellipsoidal inclusion, Comput. Mater. Sci. 231 (2024) 112568.
[31] K. Horikawa, A. Ishii, Effect of purity on the internal morphology of blisters on aluminum surfaces, Res. Mater. 21 (2024) 100522.
[32] A. Ishii, *Ab* initio morphology prediction of Zr hydride precipitates using atomistically informed Eshelby's ellipsoidal inclusion, Comput. Mater. Sci. 211 (2022) 111500.
[33] A. Ishii, Elastic investigation for the existence of B33 phase in TiNi shape memory alloys using atomistically informed Eshelby's ellipsoidal inclusion, Comput. Mater. Sci. 218 (2023) 111954.
[34] A. Ishii, Ab Initio Stability Prediction of β Titanium and α and ω Precipitates in β Titanium Matrix for Titanium Alloys Using Density Functional Theory and Micromechanics, Mater. Today Comm. 38 (2024) 107708.